JOURNAL OF SOLID STATE CHEMISTRY 63, 129–138 (1986)

New Oxyborates in the Mg–Mn–B–O System

J. J. COOPER AND R. J. D. TILLEY

Department of Metallurgy and Materials Science, University College, Newport Road, Cardiff CF2 1TA, United Kingdom

Received May 31, 1985

Two new oxyborate compounds were synthesized during a study of the phase relationships between the pinakiolite–ludwigite series of compounds. The structural topologies of these previously unreported materials have been determined experimentally by comparing calculated with observed electron microscope images. Both of these structures are very similar to each other, and also closely related to pinakiolite which consists of flat walls of edge-sharing octahedra connected to zigzag chains of octahedra by triangular BO_3 groups. The two new structures contain similar infinite walls which are separated by slabs of octahedra that are wider than the zigzag chains found in pinakiolite. A new series of structurally related oxyborate compounds can be envisaged and are described.

Introduction

The pinakiolite–ludwigite structural series found in the Mg–Mn–B–O system can be derived by periodic twinning of the idealized pinakiolite structure. Each member of this family has a unique twin repeat distance which governs the size of one axis of the unit cell. Previous studies of the synthetic and mineral compounds in this system have been largely concerned with the characterization of crystal structures and associated structural defects. For example, the synthetic and natural magnesium–mangenese borates reported by Bovin and O'Keeffe (*1*) and Bovin, O'Keeffe, and O'Keefe (*2, 3*) were found to contain numerous planar faults corresponding to variations in the twin repeat distance. This disorder often resulted in single crystals possessing several coherently intergrown structures from within the pinakiolite–ludwigite family of minerals.

These irregularities were tentatively attributed to localized differences in ionic distributions, suggesting that chemical variation is responsible for stabilization of each particular structure within the series. Experiments to fully define the relationships between structure and composition in this family of compounds were undertaken to explore the validity of this viewpoint. During this study several samples were synthesized which contained new materials. The structures of two of these are reported in this paper.

Experimental

The material under investigation was prepared by heating appropriate quantities of MgO, Mn_3O_4, and B_2O_3. The boric oxide used was reported to have a water content of less than 200 ppm. Samples were formed into pressed pellets after prolonged mixing of the oxide starting materials in an agate

0022-4596/86 $3.00

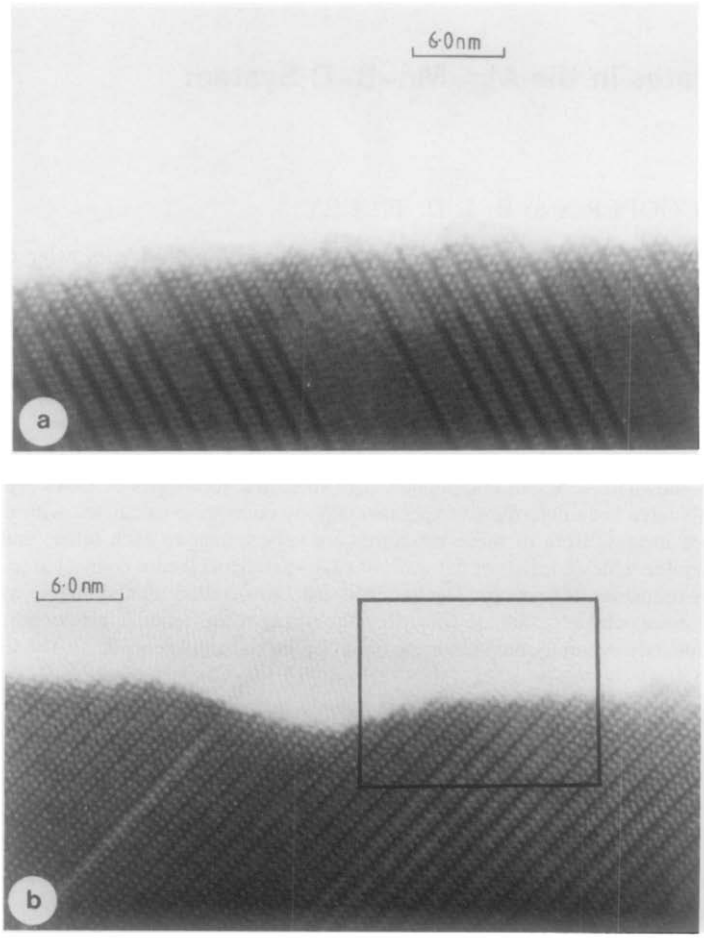

FIG. 1. (a) Typical electron micrograph of the disordered material under investigation. At the edge of the crystal the image consists of rows of white spots separated by dark bands of different intensity. (b) Electron mirograph of a crystal fragment with less disorder than Fig. 1a. The two types of image seen extend over considerable areas of the crystal and produce complex electron diffraction patterns such as Fig. 2.

mortar. These pellets were then sealed in platinum tubes and heated at 1000°C for 7 days followed by quenching into liquid nitrogen. Small amounts of the resulting materials were examined in a JEOL 200CX transmission electron microscope. For this, samples were prepared by crushing under *n*-butanol. A drop of the suspension produced in this manner was placed on a holey carbon film and allowed to dry.

Electron microscope images were obtained by precisely aligning the thin edges of crystals so that the electron beam was parallel to the short unit cell axis. Several through focal series were recorded after initially obtaining the exact focus at the edge of the crystal. Successive images were then recorded at 6-nm increments of defocus. All images were photographed at a magnification of 1,000,000× with the microscope operated at 200 kV. The objective lens had a C_s of 1.2 mm and the objective aperture

which was used to exclude reflections with large scattering angles had a radius of 3.1 nm^{-1} in reciprocal space.

The computed images were calculated on the Joint Cardiff Computing Service's Honeywell, DPS-8/70M computer, employing programs FCOEFF and DEFECT written by Skarnulis (*4*). Image calculations were performed using the 19 beams which contributed to the real micrographs and various crystal thicknesses. The depth of focus due to chromatic aberration was assumed to be 20 nm. Atomic scattering factor coefficients for the relevant ionic species were taken from "International Tables for X-Ray Crystallography," Volume IV, Table 2.2B. Images were calculated over a range of defocus of 0–100 nm.

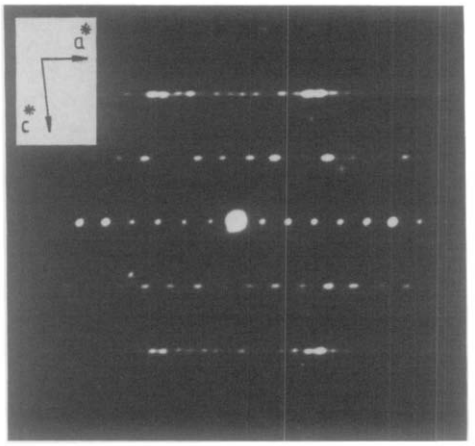

FIG. 2. Electron diffraction pattern from a highly disordered crystal. Absences appear to be evident in the central $h00$ and nearest neighboring $h01$ and $h0\bar{1}$ rows of diffraction maxima.

Results

Two previously unreported structures were observed in several samples produced by firing mixtures close to MgO + $0.75Mn_3O_4$ + $0.33B_2O_3$. Many crystal fragments from the resulting materials were observed in the electron microscope and most were easily identified from their associated electron diffraction patterns as being either spinel or ludwigite type compounds. The remainder of crystals were found to possess highly disordered structures and gave complex electron micrographs such as that given in Fig. 1a. Somewhat better ordered crystals were sometimes observed as can be seen in Fig. 1b which shows intermittent regions of different image contrast.

Diffraction Patterns

Diffraction patterns from disordered fragments were inevitably complex as can be seen in Fig. 2. At first sight, it appears that as well as a high degree of disorder giving rise to pronounced streaking of the diffraction maxima, many reflections are in fact absent from the central and nearest neighboring rows. These apparent absences are of the types $h00$ whenever h is odd and $h0l$ whenever l is odd and h is even. No combination of symmetry operators can give rise to these absences alone in the $h0l$ reciprocal lattice net, which indicates that the overall diffraction pattern was produced by more than one phase.

Closer examination of the diffraction pattern shown in Fig. 2 reveals that the $h02$ row of diffraction maxima are not spaced at regular intervals but grouped together in pairs. Also, the spots found in the $h01$ row are distinctly oval whereas those found in the $h00$ row are actually round. These facts imply that two closely related unit cells within the same crystal fragment are giving rise to the diffraction pattern and the oval shaped spots in the $h01$ row are possibly produced by two unresolved diffraction maxima.

This idea was confirmed by Fig. 3 which shows a diffraction pattern from a crystal fragment photographed using a low incident beam intensity. In this figure it is clearly seen that the overall diffraction pattern consists of two reciprocal lattice sections produced by reflections from two phases

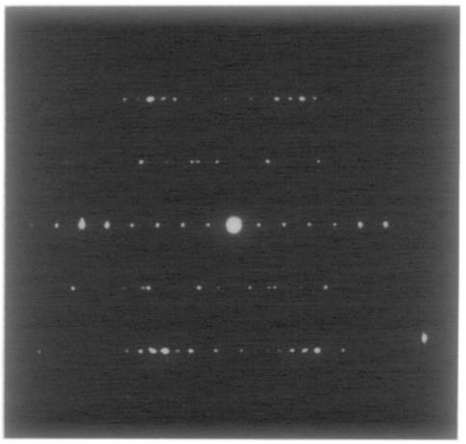

FIG. 3. Electron diffraction pattern similar to Fig. 2 but recorded with a low incident beam intensity. Note that the oval shaped spots in the $h01$ and $h0\bar{1}$ rows of diffracted beams are revealed as two distinct maxima.

with axes at slightly different angles. For clarity this situation is modeled in Fig. 4 showing the pattern produced by the two superimposed reciprocal lattice unit cells.

Careful measurement of electron diffraction patterns yields two unit cells with approximate dimensions $a = 0.6$ nm, $b = 0.6$ nm, $c = 1.5$ nm, $\beta = 96°$ and $a = 0.6$ nm, $b = 0.6$ nm, $c = 1.5$ nm, $\beta = 105°$.

Interpretation of Image Contrast

The interpretation of image contrast in terms of crystal structure is often very difficult and when the crystal structure of the material in question is unknown, considerable care must be taken when extrapolating from electron micrographs to possible structure. This task is, however, made easier if the unknown structure is coherently intergrown with a phase of known structure (*4*). In such a case the material can be imaged so that the contrast in the areas corresponding to the known structure can be directly related to known crystallographic features. Ideally, this means that one obtains images where dark contrast corresponds to positions of high electron density, i.e., atom positions. With this achieved, it is then possible to say, with reasonable confidence, that similar contrast in the adjacent areas of the new phase can be interpreted in an analogous fashion. These images can then be used to deduce plausible structural models of the unknown phase or phases.

This technique was used as a first step in solving these two new structures. The two types of image contrast shown in Fig. 1 show close similarities to the high-resolution electron micrographs of the mineral pinakiolite reported by Bovin, O'Keeffe, and O'Keefe (*2*). In Fig. 1, at the very edge of the crystal, the image consists of rows of white spots grouped in pairs separated by two types of dark wall of differing intensity but similar widths. Pinakiolite micrographs produced by the workers above and by ourselves also consist of double rows of white spots separated by dark walls, corresponding to zigzag chains of octahedra, slightly smaller in width than those recorded in Fig. 1. In fact, Fig. 5 contains a fault in which the image contrast exactly matches these pinakiolite micrographs and shows a direct correspondence to the idealized structure reproduced in the inset polyhedral diagram.

Taking the structure of pinakiolite as known and then using the contrast in Fig. 5,

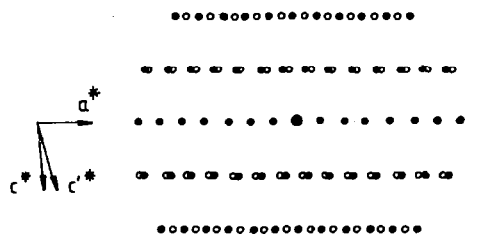

FIG. 4. Diagramatic representation of the particular intensity distributions in Figs. 2 and 3. These electron diffraction patterns are believed to be produced by the superposition of the two reciprocal lattice nets. The two sets of diffraction spots involved are given as shaded and light circles which coincide in the $h00$ row and partially overlap in the $h01$ and $h0\bar{1}$ rows.

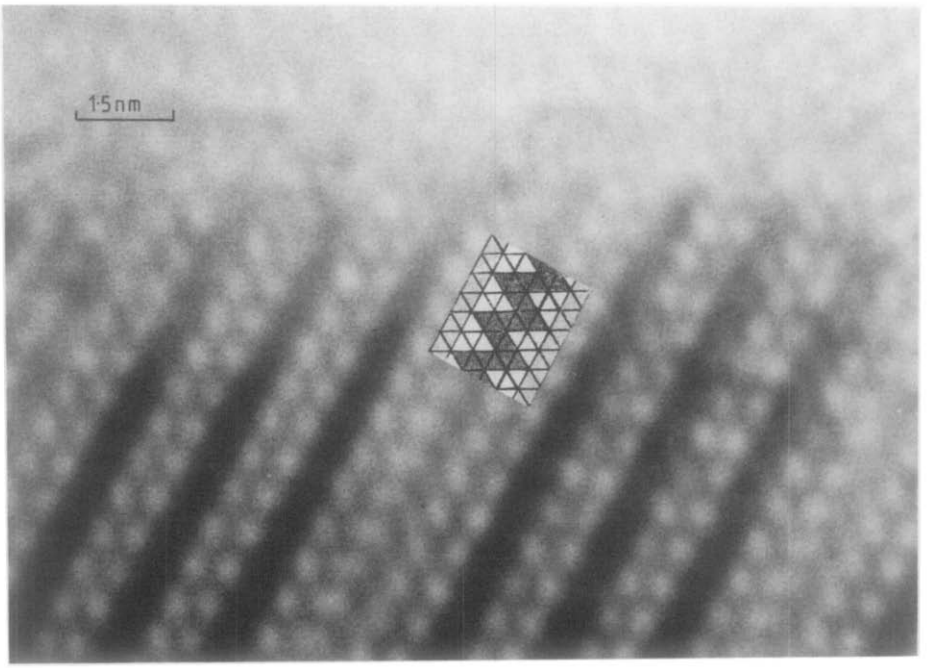

FIG. 5. Electron micrograph which contains a fault with image contrast that directly corresponds to the inset polyhedral diagram of the pinakiolite structure and also matches the electron microscope images of pinakiolite produced by Bovin *et al.* (2).

for example, as a guide, the structure of the new phases can be deduced. It is immediately clear that both structures have a close similarity to pinakiolite since the only obvious difference between the images of pinakiolite and Fig. 1 is that the dark zigzag chains are replaced by two different types of broader bands.

Several plausible structural models for the two new structures have been considered. These models were all closely related to the pinakiolite structure but could contain either broader zigzag chains or wider flat walls of edge sharing octahedra connected by planar triangular boron–oxygen groups. Two of these structures (designated structure 1 and structure 2) are shown in Fig. 6, together with the structure of pinakiolite for comparison.

In Fig. 6 the cation-centered octahedra share edges and corners to form different types of walls or slabs which are connected alternately by corner sharing. The structural similarity of pinakiolite with these two models is obvious. In the two models the pinakiolite zigzag chains are replaced by wider slabs of material containing a greater number of ions. The difference between structure 1 and structure 2, given in Figs. 6b and c, respectively, can be envisaged by considering the ways in which the two types of wall can affix themselves to one another. In structure 1 they are arranged in such a manner that the unit cell projection shown is rectangular. However, if the octahedra on the right side of the central wall are displaced by one octahedral edge distance in the direction indicated, then a new structure is generated. To produce the second unit cell in which only the indicated angles α and β are not equal to 90° it is necessary to arrange the flat walls of

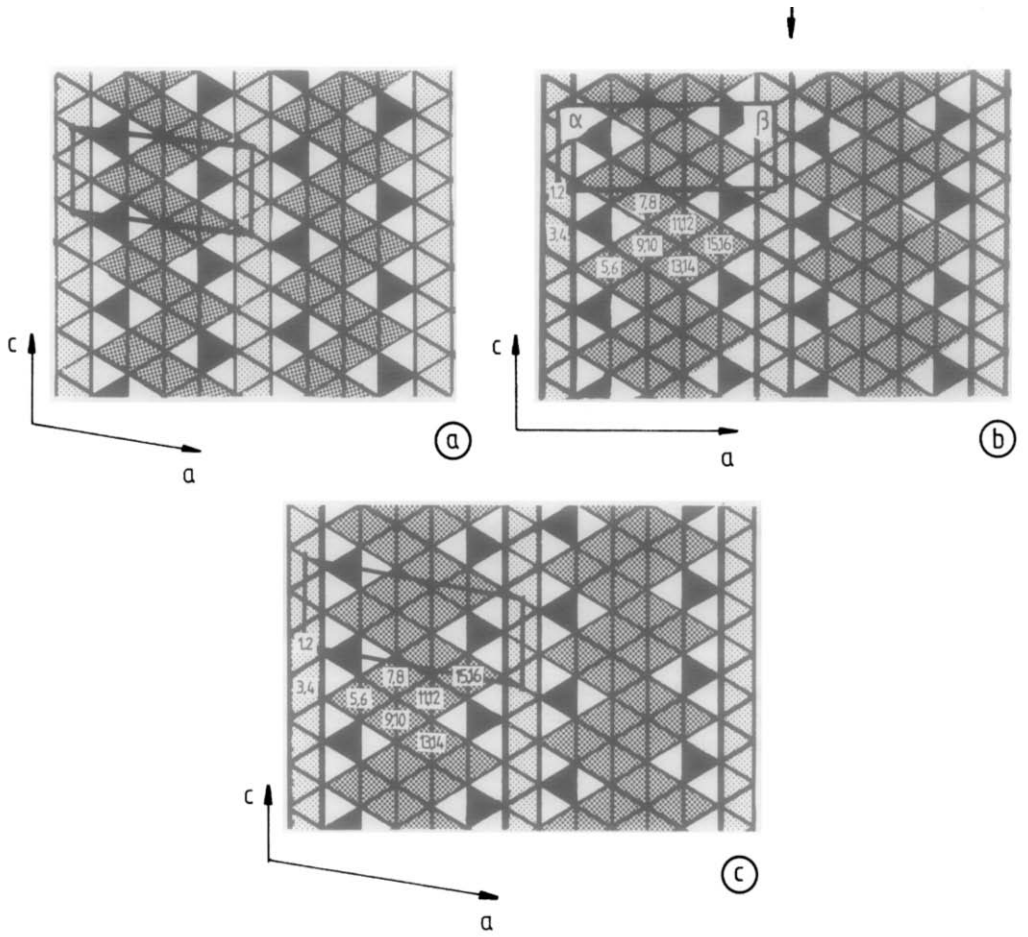

FIG. 6. Idealized diagrams of the pinakiolite structure (a) and the proposed structures for the two new phases observed. Both structure 1 (b) and structure 2 (c) are very similar to pinakiolite but with the zigzag chains of octahedra replaced by larger slabs of material with the close packed rock salt-like structure.

octahedra in the opposite orientation to those in structure 1. This requirement occurs since the displacement shown also gives rise to a shift parallel to the *b* axis of the unit cell given in Fig. 6b. Clearly, both structures seem equally plausible since no lattice distortions or changes in composition occur in the above process.

The structures so produced give rise to diffraction patterns which are in qualitative agreement with those obtained experimentally, that is, the spot positions are correct. At this juncture we have not yet computed the intensities of these reflections.

Image Calculations

According to present theory, the best correspondence between the actual structure and contrast in both real and calculated images should occur at an underfocus of approximately −100 nm. However, many difficulties arise in image matching even

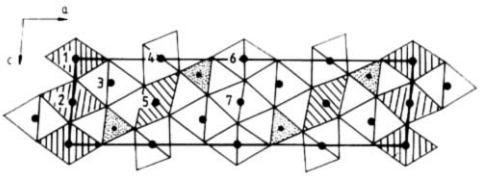

FIG. 7. Polyhedral diagram of the real pinakiolite structure with the Mn^{3+}–O octahedra ruled. The remaining unshaded polyhedra are occupied by both Mg and Mn^{2+} except those labeled (3) which are entirely filled by Mg. The triangular BO_3 groups are shown stippled.

when the structure is known. For example, it is difficult to estimate the thickness of the crystal being studied and the exact extent of underfocus of the microscope. Hence it is necessary to vary both of these parameters when comparing real and calculated micrographs to produce several series of computed images. To ensure that an approximate structure determination has been performed, at least one series must show a direct correspondence to the actual images over a range of defocus of several tens of nanometers, and not in just one or two isolated instances.

The ionic coordinates required for the calculation of microscope images were modeled on those found in pinakiolite. The ionic ordering scheme in pinakiolite, as determined by Moore and Araki (*5*), is shown in Fig. 7 and is such that most of the octahedra in the *b* axis direction are alternately occupied by either Mg or Mn. The exceptions to this rule are the cation sites labeled M(3) which are fully occupied by Mg. By the same analogy the octahedra in the two new structures were filled in a similar manner except those found at the extremes of the larger slabs which attach to the narrower walls by corner sharing. These cation sites, designated M(4), M(5), M(15), and M(16), were completely filled by Mg ions as is the case with "equivalent" sites marked M(3) in pinakiolite. The metal ion coordinates produced in this manner for structures 1 and 2 are given in Tables I and II, respectively.

TABLE I

POSITIONAL PARAMETERS FOR THE METAL CATIONS IN STRUCTURE 1

Atom	*X*	*Y*	*Z*
Mg(1)	0.0	0.0	0.0
Mn^{2+}(2)	0.0	0.5	0.0
Mn^{2+}(3)	0.0	0.25	0.5
Mg(4)	0.0	0.75	0.5
Mg(5)	0.25	0.25	0.125
Mg(6)	0.25	0.75	0.125
Mg(7)	0.417	0.0	0.875
Mn^{3+}(8)	0.417	0.5	0.875
Mg(9)	0.417	0.0	0.375
Mn^{3+}(10)	0.417	0.5	0.375
Mn^{3+}(11)	0.584	0.25	0.625
Mg(12)	0.584	0.75	0.625
Mn^{3+}(13)	0.584	0.25	0.125
Mg(14)	0.584	0.75	0.125
Mg(15)	0.75	0.0	0.375
Mg(16)	0.75	0.5	0.375

For these two idealized models the units cell dimensions, as determined from an octahedral edge distance of 0.3 nm are $a = 0.6$

TABLE II

POSITIONAL PARAMETERS FOR THE METAL CATIONS IN STRUCTURE 2

Atom	*X*	*Y*	*Z*
Mg(1)	0.0	0.0	0.0
Mn^{2+}(2)	0.0	0.5	0.0
Mn^{2+}(3)	0.0	0.25	0.5
Mg(4)	0.0	0.75	0.5
Mg(5)	0.25	0.0	0.5
Mg(6)	0.25	0.5	0.5
Mg(7)	0.417	0.25	0.833
Mn^{3+}(8)	0.417	0.75	0.833
Mg(9)	0.417	0.25	0.333
Mn^{3+}(10)	0.417	0.75	0.333
Mn^{3+}(11)	0.584	0.0	0.667
Mg(12)	0.584	0.5	0.667
Mn^{3+}(13)	0.584	0.0	0.167
Mg(14)	0.584	0.5	0.167
Mg(15)	0.75	0.25	0.0
Mg(16)	0.75	0.75	0.0

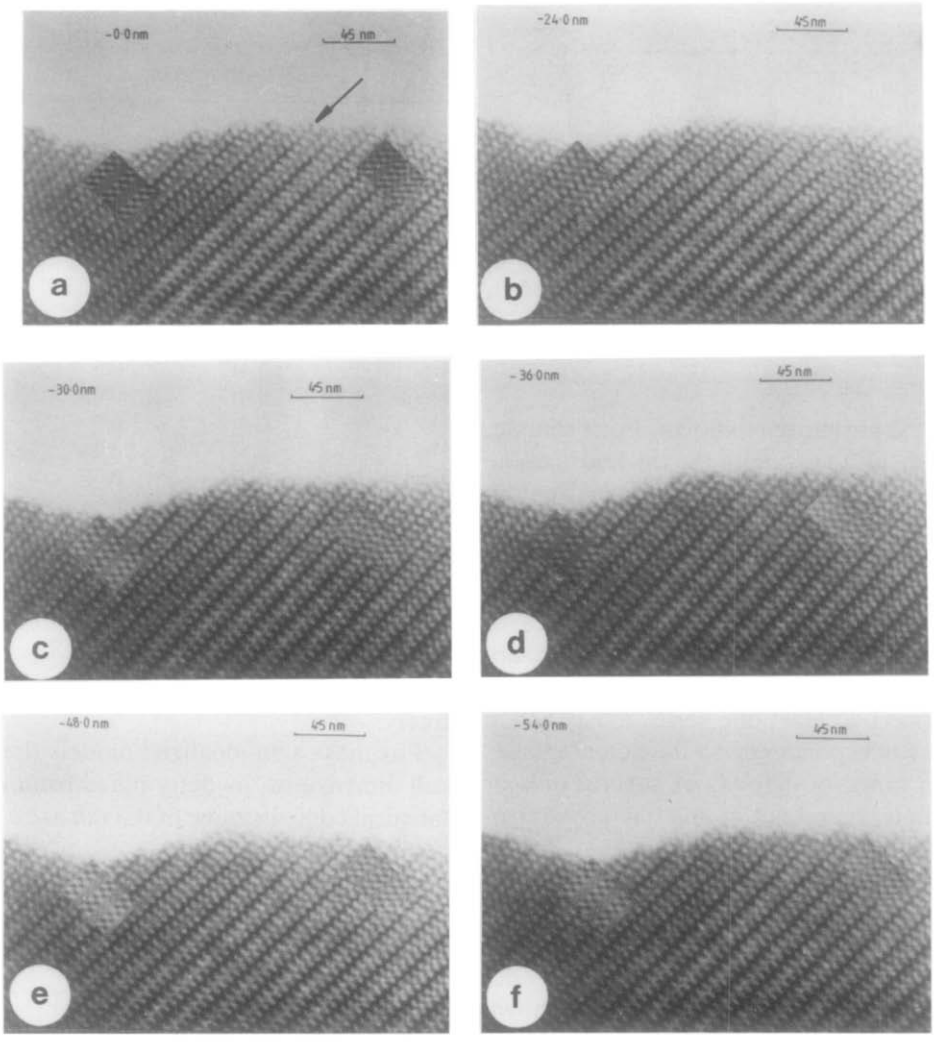

FIG. 8. Through focal series of electron micrographs from the area marked in Fig. 1b. Both types of image are visible with the boundary between the two marked in (a). The inset calculated images on the left and right side of each micrograph were generated from structures 1 and 2, respectively. Each series matches the real image contrast over a wide range of defocus.

nm, $b = 0.6$ nm, $c = 1.56$ nm for structure 1 and $a = 0.6$ nm, $b = 0.6$ nm, $c = 1.59$ nm, $\beta = 100.9°$ for structure 2. These two sets of unit cell data compare quite favorably with those calculated from the observed diffraction patterns, especially when one considers that the samples contain the Jahn-Teller ion Mn^{3+} which is known to produce quite severe geometrical distortions in these oxyborate compounds and many other oxides. For the image calculations the measured unit cell dimensions were employed instead of those calculated from the idealized models.

In the micrographs the extent of defocus was determined by first focusing at the very edge of the crystal to obtain the position of minimum contrast in the contaminated ar-

eas seen in Fig. 1b. A through focal series was then recorded along with the position of the fine focus control of the microscope. The micrographs in Fig. 8 represent such a series from the area indicated in Fig. 1b. The inset matching computed images were produced at the same degree of defocus using a crystal thickness of 3.0 nm.

This series of electron micrographs shows a structural change across the boundary marked in Fig. 8a which is revealed by differences in image contrast on either side of it. Good agreement between the two sets of calculated and experimental images indicates that the left side of crystal possesses the idealized structure in Fig. 6b and the right side, the second structure shown in Fig. 6c. This image matching sequence clearly reveals that at the thin edges the white spots correspond to the boron atom positions of low electron density and the walls of the octahedra show up in the micrographs as broad gray bands.

Discussion

The results reported here represent an approximate structure determination of two previously unreported phases. It must be remembered that the two proposed structures are, however, idealized since the large number of distinguishable ways in which the Mg and Mn ions can be distributed over the available octahedral sites has not yet been explored. Even so, it is believed that the two structures have been deduced in terms of coordination polyhedra since there exists a direct correspondence between the experimental images and the calculated images through a range of defocus of more than 50 nm.

The structures themselves are similar to pinakiolite, but with wider slabs of zigzag structure between the straight walls of octahedra. This zigzag region can be thought of as consisting of a ribbon of rock salt structure type. We can therefore regard the phases as being coherent intergrowths of slabs of rock salt, MO, where M could be Mg, Mn, or a mixture of both, with slabs of the pinakiolite structure. The two phases described here have the same stoichiometry and differ only because the linkage between the straight walls and the zigzag strips can be made in two ways.

Clearly as a result of this work, a whole new family of oxyborate compounds can be visualized with pinakiolite as the first member in the series and rocksalt as the final member. The idealized stoichiometry of pinakiolite can be regarded as M_3BO_5, $MO_{1.25}$, where M stands for mainly Mg^{2+}, Mn^{2+}, and Mn^{3+}. Similarly, the two new structures contain these cations in such a ratio that gives to the overall formula M_4BO_6, i.e., $MO_{1.2}$. The difference in composition, by the amount MO, is brought about during the formation of these materials by accommodation of extra metal–oxygen octahedra in the pinakiolite zigzag chains. One can then envisage a series of structures, with even wider walls of edge-sharing octahedra, in which the composition sequence is given by $M_{3+x}BO_{5+x}$ (where $x = 1,2,3, \ldots$). For example, Fig. 9 shows two possible structures for the next step within this series which would both have the same composition, namely M_5BO_7, or $MO_{1.167}$.

In the foregoing discussion, the structures have been treated as slabs of rock salt type, MgO or MnO, intergrown with elements of the pinakiolite structure. Of course, within the rocksalt structure, all of the tetrahedral sites are empty and all of the octahedral sites are full. The spinel structure is very simlar to the rocksalt structure, except that the cations are now distributed over both octahedral and tetrahedral sites, and the stoichiometry is now M_3O_4. Our electron micrographs do not, in fact, allow us to distinguish between zigzag regions which are strictly rocksalt or those which are spinel in structure. Consequently an

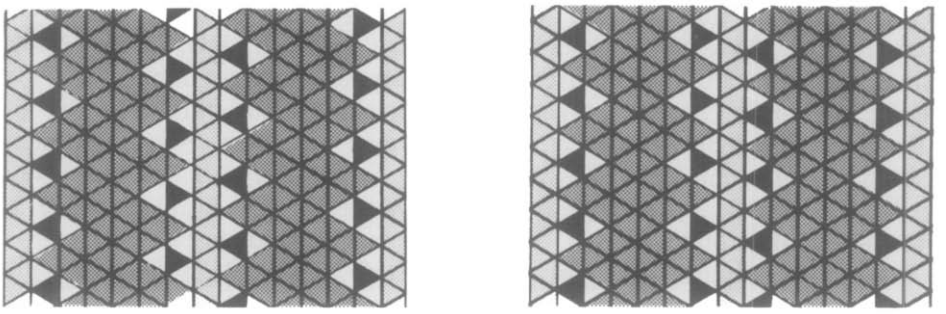

FIG. 9. Idealized polyhedral diagrams for two hypothetical structures produced when even wider slabs of edge sharing octahedra replace the zigzag chains found in the pinakiolite structure.

analogous series of structures with spinel-like slabs of material may form. These will have a different series formula than that given above, and lie between the composition limits of pinakiolite, $MO_{1.25}$, and spinel $MO_{1.33}$. For the moment we will not consider this series further but note that if structures with wider zigzag strips can be prepared, we should be able to differentiate between these two possibilities.

At present, further experiments to determine the exact composition of the new structures are being performed with the aim of producing single phase materials for study by X-ray diffraction. Along with this work, reactions which will hopefully result in the synthesis of higher members of this hypothetical series are now underway and will be reported in the future.

Acknowledgment

J. J. Cooper is indebted to ICI plc for financial support.

References

1. J. O. BOVIN, M. O'KEEFFE, *Acta Crystallogr. Sect. A* **37,** 35 (1981).
2. J. O. BOVIN, M. O'KEEFFE, AND M. A. O'KEEFE, *Acta Crystallogr. Sect. A* **37,** 28 (1981).
3. J. O. BOVIN, M. O.'KEEFFE, AND M. A. O'KEEFE, *Acta Crystallogr. Sect. A* **37,** 42 (1981).
4. G. VAN TENDELOO, D. VAN DYCK, J. VAN LANDUYT, AND S. AMELINCKX, *J. Solid State Chem.* **27,** 55 (1979).
5. P. B. MOORE AND T. ARAKI, *Am. Mineral.* **59,** 985 (1974).
6. A. J. SKARNULIS, Ph.D Thesis, Arizona State University, 1978.